# Letters

## Physics-Based SPICE Modeling of Dynamic ON-State Resistance of p-GaN HEMTs

Sheng Li, Yanfeng Ma, Chi Zhang, Weihao Lu, Mengli Liu, Mingfei Li, Lanlan Yang, Siyang Liu, *Member, IEEE*, Jiaxing Wei, *Member, IEEE*, Long Zhang, *Member, IEEE*, Weifeng Sun, *Senior Member, IEEE*, and Jiaxin Sun

***Abstract*—This letter introduces a new physics-based SPICE modeling method for the dynamic ON-state resistance ($R_{\mathrm{on,dy}}$) of gallium nitride based p-type gate power high electron mobility transistors (p-GaN HEMTs). To describe the continuous variations of $R_{\mathrm{on,dy}}$, a time-resolved electron mobility variation ($\Delta\mu_{\mathrm{eff}}$) model is proposed. Physical parameters including activation energy and voltage acceleration factor of traps in p-GaN HEMTs are extracted as the model parameters. Then, to achieve the goal of simulating $R_{\mathrm{on,dy}}$, the proposed $\Delta\mu_{\mathrm{eff}}$ model is incorporated into the surface potential based advanced SPICE model for GaN HEMT. Simulative results prove the proposed models can predict the $R_{\mathrm{on,dy}}$ induced power loss.**

***Index Terms*—Dynamic $R_{\mathrm{on}}$, p-type gate power high electron mobility transistor (p-GaN HEMT), SPICE model.**

### I. Introduction

GALLIUM-nitride-based power high electron mobility transistors with p-type gate cap (p-GaN HEMTs) have exhibited superiorities of high frequency, high power density, and high breakdown voltage in power electronic systems [1], [2], [3]. However, since the p-GaN HEMTs are fabricated based on heteroepitaxy process, many traps are introduced into the bulk and materials. It is hard to inhibit the generations of these traps thoroughly, hence resulting in dynamic ON-state resistance ($R_{\mathrm{ON,dy}}$) phenomenon during switching operations [4], [5], [6], [7], [8]. The p-GaN HEMTs with $R_{\mathrm{ON,dy}}$ will lead to conduction loss, temperature rise, even failure of power electronic systems [9]. The influences of $R_{\mathrm{ON,dy}}$ should be considered when designing power systems, unfortunately, the conventional SPICE models which are used by designers cannot describe $R_{\mathrm{ON,dy}}$. Thus, the development of GaN HEMT SPICE model that describes $R_{\mathrm{ON,dy}}$ is required.

According to the mechanisms behind $R_{\mathrm{ON,dy}}$, the modeling of trapping effect is essential to describe $R_{\mathrm{ON,dy}}$ [10]. The resistance–capacitance (RC) networks are widely used in previous investigations to model trapping effect. Accordingly, some SPICE models are proposed to describe $R_{\mathrm{ON,dy}}$ by adding RC networks to gate or drain terminals [11], [12], [13], [14]. Those works could be very useful in power electronic system design. However, to further improve the model accuracy, more physics-based SPICE models that describe $R_{\mathrm{ON,dy}}$ are required. For previous models based on RC networks, multiple stage RC networks are required to improve the accuracy, hence, the numbers of model parameters are increased. It could be a challenge to extract a lot of appropriate model parameters. Thus, new approaches are highly required to build physics-based compact SPICE models including $R_{\mathrm{ON,dy}}$ descriptions.

In this letter, a new approach which is based on electron mobility variation is proposed to describe trapping-induced $R_{\mathrm{ON,dy}}$ phenomenon; meanwhile, the essential model parameters are physical and extracted by experiments. Furthermore, the model is incorporated into surface potential based advanced SPICE model for GaN HEMT (ASM-HEMT). In this way, the proposed model is available for $R_{\mathrm{ON,dy}}$ simulations.

### II. Methodologies

#### A. Characterizations of $\mathrm{R_{on,}}_{dy}$

Accurate $R_{\mathrm{ON,dy}}$ characterizations should be accomplished before the modeling job. High-voltage stress is necessary to active the $R_{\mathrm{ON,dy}}$, the stress magnitude and stress time should be controlled accurately to meet the requirements of high accuracy of modeling. Therefore, the circuit shown in Fig. 1(a) is adopted to measure $R_{\mathrm{ON,dy}}$ [14], [15]. In this circuit, the stress magnitude is controlled by $V_{\mathrm{bus}}$ and the stress time is controlled by $T_1$.

Manuscript received 17 December 2022; revised 4 March 2023; accepted 26 March 2023. Date of publication 29 March 2023; date of current version 19 May 2023. This work was supported in part by the National Natural Science Foundation of China under Grant 62204034 and Grant 62174029; in part by the China Postdoctoral Science Foundation under Grant 2022TQ0061 and Grant 2022M720710; and in part by the Key Research Program of Jiangsu Province under Grant BE2022058-3. *(Corresponding authors: Siyang Liu; Weifeng Sun.)*

Sheng Li, Yanfeng Ma, Chi Zhang, Weihao Lu, Mengli Liu, Mingfei Li, Siyang Liu, Jiaxing Wei, Long Zhang, and Weifeng Sun are with the National ASIC System Engineer Research Center, Southeast University, Nanjing 210096, China (e-mail: seulisheng@seu.edu.cn; 220205822@seu.edu.cn; galazhang@seu.edu.cn; 220205882@seu.edu.cn; liuml18317869002@163.com; mingfly2020@outlook.com; liusy2017@seu.edu.cn; jiaxingwei@seu.edu.cn; longzh@seu.edu.cn; swffrog@seu.edu.cn).

Lanlan Yang is with the National Center of Technology Innovation for EDA, Southeast University, Nanjing 210096, China (e-mail: jujube_yang@seu.edu.cn).

Jiaxin Sun is with the Julin Tech. Co. Ltd., Shanghai 201210, China (e-mail: jiaxinsun@julin-tech.com).

Color versions of one or more figures in this article are available at https://doi.org/10.1109/TPEL.2023.3262938.

Digital Object Identifier 10.1109/TPEL.2023.3262938

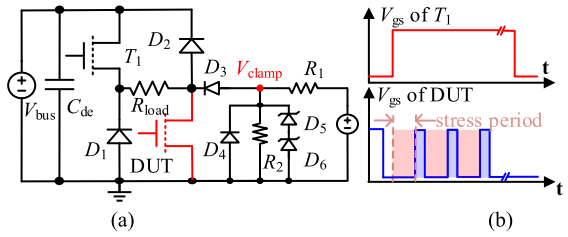


Fig. 1. Characterization of $R_{\mathrm{ON,dy}}$: (a) test circuit and (b) control signals.

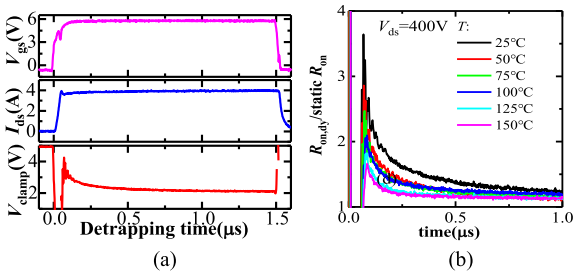


Fig. 2. Characterization results of $R_{\mathrm{ON,dy}}$: (a) measured waveforms of using above test circuit and (b) extracted $R_{\mathrm{ON,dy}}$.

When $T_1$ is turned OFF, $V_{\mathrm{bus}}$ drops on $T_1$ and the device under test (DUT) is unstressed. When $T_1$ is turned ON and DUT is turned OFF, $V_{\mathrm{bus}}$ drops on DUT and DUT is stressed. Once this period is set, the stress time of DUT is controlled. Meanwhile, the monitored voltage is the clamp voltage of the clamp circuit, which is a small value. When $T_1$ and DUT are turned ON at the same time, the monitored voltage equals to the voltage drop on DUT and $D_3$, where $D_3$ should be a diode that withstands high voltage like $D_2$. In this way, the $R_{\mathrm{ON,dy}}$ can be measured accurately with the help of clamp circuit. The above processes describe a single pulse measurement; however, $R_{\mathrm{ON,dy}}$ evaluation under continuous-pulse conditions are necessary considering practical working scenes. In this circuit, when $T_1$ is turned ON, $R_{\mathrm{ON,dy}}$ characterizations under continuous-pulse working conditions can be also achieved by giving DUT continuous-pulse signals. The typical measured waveforms under single pulse conditions are shown in Fig. 2(a), the typical extracted $R_{\mathrm{ON,dy}}$ waveforms under different stress magnitudes and temperatures are shown in Fig. 2(b).

### B. Derivation of Models

As reported, trapping effect near channel layer could change the charge density near channel layer, hence introducing scattering effect and changing the effective electron mobility ($\mu_{\mathrm{eff}}$) in channel [16], as shown in Fig. 3(a). Finally, $R_{\mathrm{ON,dy}}$ is observed. Based on this mechanism, $R_{\mathrm{ON,dy}}$ can be described by modeling the variations of $\mu_{\mathrm{eff}}$. During stress process, trapping-induced scattering effect is enhanced and the $\mu_{\mathrm{eff}}$ is reduced correspondingly, once the stress is withdrawn, the scattering effect is mitigated and the $\mu_{\mathrm{eff}}$ is recovered gradually. Considering the correlation between the variation of $\mu_{\mathrm{eff}}$ and trapping effect, $\mu_{\mathrm{eff}}$ can be modeled using models that describe trapping effect. Due

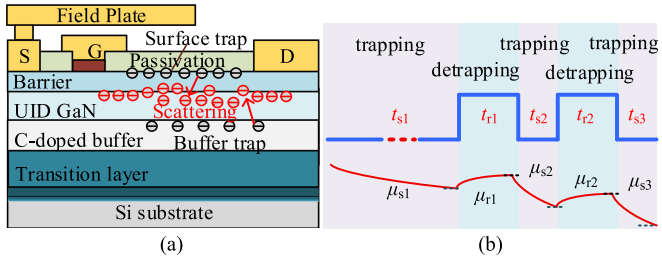


Fig. 3. Degradation mechanisms of $R_{\mathrm{ON,dy}}$. (a) Sketch of the trapping effect. (b) Sketch of the time-resolved variations of $\mu_{\mathrm{eff}}$.

to the fact that the bias conditions during trapping period are different from those during detrapping period, the trapping and detrapping processes should be modeled separately. For trapping process, (1) is deducted from Arrhenius equation to build the $\mu_{\mathrm{eff}}$ model [17], where $E_{a,s}$ is the activation energy of traps, $k$ is boltzmann constant, $T$ is temperature, $V_s$ is stress voltage, $\beta_s$ is the acceleration factor of $V_s$, $t_s$ is stress time, and $n$ is an exponential parameter. The scattering-dependent parameters are merged into the model parameter $k_s$. For detrapping process, (2) is deducted from a normal exponential function, where $t_r$ is recovery time and $\tau_r$ is time constant of detrapping process.

Since the $\mu_{\mathrm{eff}}$ cannot be recovered to the initial value $\mu_0$ in time after each trapping and detrapping cycles, $\mu_{\mathrm{eff}}$ should be updated instantly at a certain moment under continuous working condition. In other word, to build the $R_{\mathrm{ON,dy}}$ models for continuous-pulses working condition, the variations of $\mu_{\mathrm{eff}}$ should be time-resolved, as shown in Fig. 3(b). Based on the trapping and detrapping models shown in (1) and (2), $\mu_{\mathrm{eff}}$ in stress period $t_{s1}$ can be modeled as (3), while $\mu_{\mathrm{eff}}$ in recovery period $t_{r1}$ can be modeled as (4). The $\Delta\mu_{\mathrm{eff}}$ in the following periods can be modeled in this manner

$$\Delta\mu_{\mathrm{trapping}}/\mu_{\mathrm{eff}} = k_s(t_s)^n V_s^{\beta s} \exp\left(\frac{E_{a,s}}{kT}\right) \tag{1}$$

$$\Delta\mu_{detrapping}/\mu_{\mathrm{eff}} = k_r \exp\left(-\frac{t_r}{\tau_r}\right) \tag{2}$$

$$\mu_{s1} = \frac{\mu_0}{1+\Delta\mu_{\mathrm{trapping}}/\mu_0} \tag{3}$$

$$\mu_{r1} = \mu_{s1}(1+\Delta\mu_{\mathrm{detrapping}}/\mu_{s1}). \tag{4}$$

For convenient applications, the deducted equations are incorporated into a SPICE model (ASM-HEMT) and a mature SPICE simulation tools (TJSPICE) [18], [19]. However, ASM-HEMT is a model for normally ON devices. To make this model available for p-GaN gate structure, the surface potential calculations for gate stack are rebuilt based on the physics of p-GaN layer. The $\mu_0$ used in (3) is the $\mu_{\mathrm{eff}}$ in ASM-HEMT. The simulation tool TJSPICE is rebuilt to link the proposed time-resolved $\Delta\mu_{\mathrm{eff}}$ model and initial $\mu_{\mathrm{eff}}$ model in ASM-HEMT. In this way, the modeling process is achieved.

### C. Extraction of Model Parameters

In the proposed models, the essential model parameters are just the trap information. Thus, the model parameters can be acquired by extracting the trap information from measured data. Some methods have been proposed to extract the information of traps that cause $R_{\mathrm{ON,dy}}$. Exponential functions (5) and (6) are adopted to describe the trapping induced increase and detrapping induced decrease of $R_{\mathrm{ON,dy}}$ [20], respectively. To extract the trap information, first, the $R_{\mathrm{ON,dy}}$ is measured under different stress magnitudes, stress times, and ambient temperatures ($T$). Then, the $\tau$ values during trapping and detrapping processes are extracted by fitting the measured data with (5) and (6). According to the relationship in (7) and the extracted $\tau$ values, the $E_a$ during trapping and detrapping processes can be deduced, respectively. Similarly, according to the extracted $E_a$ value, the $\beta$ of $V_{\mathrm{ds}}$ during trapping process and $\beta$ of $V_{\mathrm{gs}}$ during detrapping process can be deduced, respectively. Finally, $E_{a,s}$, $\beta_s$ in (1) are the $E_a$ and $\beta$ for trapping process, $\tau_r$ in (2) is deduced by (8)

$$\Delta R(t) = \Delta R_c(1 - \exp(-(t/\tau_c)^{\beta c})) \tag{5}$$

$$\Delta R(t) = \Delta R_e \exp(-(t/\tau_e)^{\beta e}) \tag{6}$$

$$\ln(\tau T^2) = m + \frac{E_a}{kT} + \beta V \tag{7}$$

$$\frac{1}{\tau_r} = \gamma_n \sigma_n T^2 \exp\left(-\frac{E_{a,r}}{kT}\right). \tag{8}$$

## III. Results and Discussions

The $R_{\mathrm{ON,dy}}$ of commercial 650 V/10 A p-GaN gate HEMT under high-voltage stresses is modeled in this letter. To extract model parameters during trapping process, $R_{\mathrm{ON,dy}}$ under different stress time, different stress magnitude, and different temperature are acquired using the circuit shown in Fig. 1, and the $R_{\mathrm{ON,dy}}$ is extracted at the moment 250 ns after the DUT is turned ON. Then, the $\tau$ for trapping process can be extracted using (5), and Fig. 4(a) and (b) presents the fitting results. To extract model parameters during detrapping process, $R_{\mathrm{ON,dy}}$ under different detrapping time, different gate to source bias, and different temperature are acquired using the circuit shown in Fig. 1, as well. Then, $\tau$ for detrapping process can be extracted using (6), and Fig. 4(c) and (d) presents the fitting results. Consequently, the essential model parameters can be deduced using (7) and (8), as shown in Fig. 5(a)-(d), respectively.

After extracting the model parameters, the proposed $\Delta\mu_{\mathrm{eff}}$ model is incorporated into the simulation tool. In this way, the static and dynamic electrical performances of p-GaN HEMT can be simulated, and the results are presented in Fig. 6. The fitting errors between simulated data and measured data of the transfer and output characteristics are 4.66% and 4.37%, respectively. A test circuit with resistive–inductive load recommended by JEDEC is adapted for characterizing $R_{\mathrm{ON,dy}}$ during continuous switching processes [21], as shown in Fig. 7(a). The fitting results of continuous switching processes are shown in Fig. 7(b) and (c). Although the $V_{\mathrm{ds}}$ is fitted well, the measured $V_{\mathrm{ds}}$ cannot be used to calculate the $R_{\mathrm{ON,dy}}$ accurately. To show the fitting

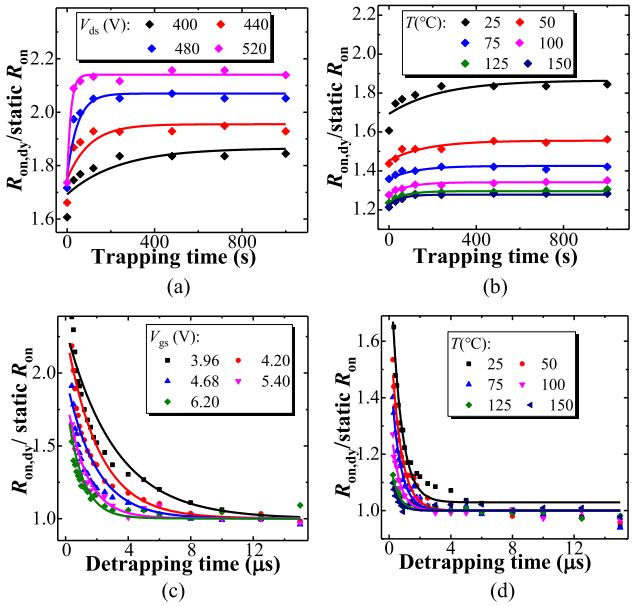


Fig. 4. Extracting $\tau$ of traps under different conditions. (a) Trapping processes as $V_{\mathrm{ds}}$ varies. (b) Trapping processes as $T$ varies. (c) Detrapping processes as $V_{\mathrm{gs}}$ varies. (d) Detrapping processes as $T$ varies.

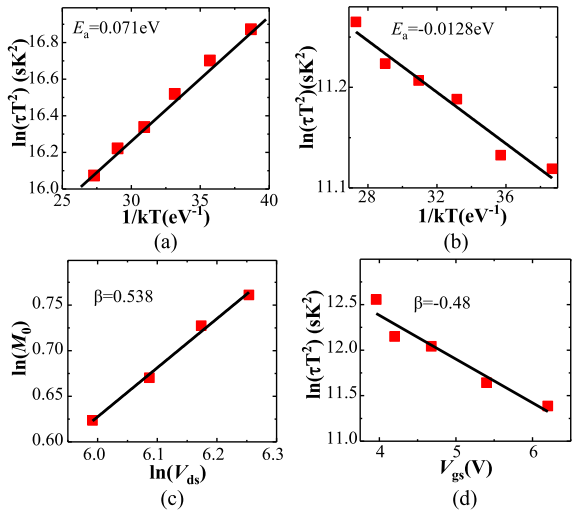


Fig. 5. Extracting model parameters. (a) $E_a$ under trapping condition. (b) $E_a$ under detrapping condition. (c) $\beta$ of $V_{\mathrm{ds}}$. (d) $\beta$ of $V_{\mathrm{gs}}$.

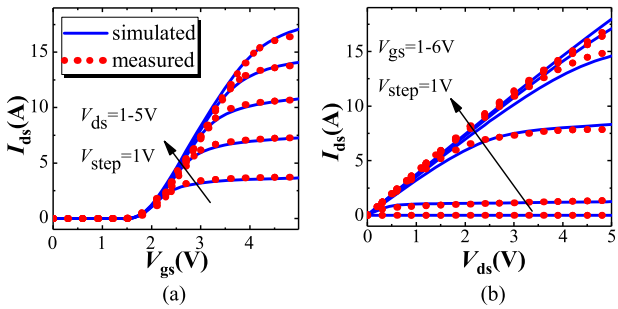


Fig. 6. Validations of static and dynamic electrical characteristics. (a) Transfer characteristics. (b) Output characteristics.

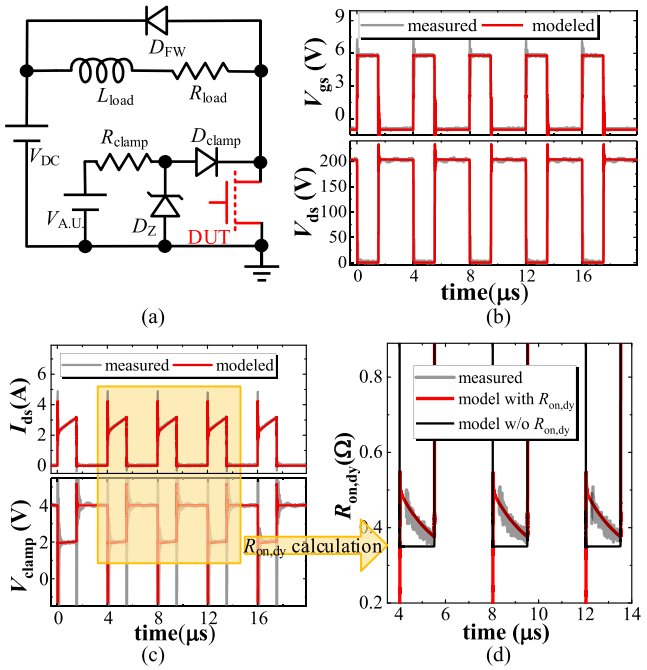


Fig. 7. Validations of Ron, dy model under continuous-pulse working condition: (a) Test circuit, (b) fitting of gate voltage and drain voltage, (c) fitting of drain current and clamp voltage, (d) fitting of calculated $R_{on,dy}$.

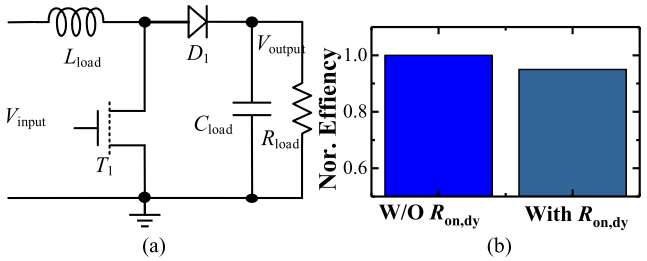


Fig. 8. Predictions of converter efficiency using proposed $R_{on,dy}$ model: (a) Circuit topology, (b) normalized efficiency.

results of $R_{ON,dy}$ intuitively, the clamp voltage is also fitted, the results prove that the voltage drop on DUT is simulated accurately, accordingly, the simulated $R_{ON,dy}$ can be extracted, as shown in Fig. 7(d). It can be observed that the $V_{ds}$ on DUT is much larger at the beginning of turn-ON transient, proving that $R_{ON,dy}$ is successfully simulated. Meanwhile, the fitting error between simulated data and measured data is calculated as 8.34%, which is smaller than that of previous works. These results indicate the proposed models successfully simulate the static and dynamic electrical performances of p-GaN HEMT.

Furthermore, the proposed SPICE model with $R_{on,dy}$ is adopted to predict the performances of a GaN based boost DC to DC converter. Fig. 8(a) is the topology of the converter, Fig. 8(b) gives the normalized simulative efficiency of the converter, it is observed that the efficiency is reduced by 5.1% due to $R_{on,dy}$ effect. However, this phenomenon may not be observed by traditional SPICE models. Hence, the superiority of the proposed SPICE models with $R_{on,dy}$ is reflected.

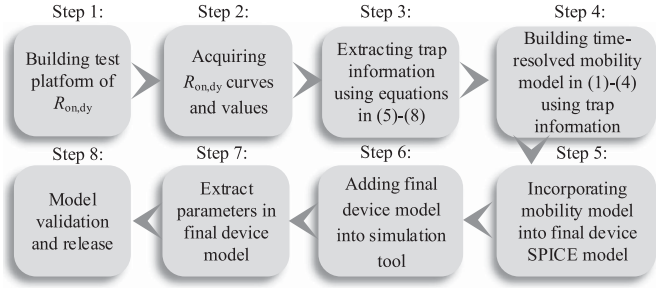


Fig. 9. Modeling procedure of the proposed method.

The general modeling procedures are concluded in Fig. 9. Among the procedures, extracting trap information using measured $R_{on,dy}$ data in Step 3 and then taking it as model parameter of the time-resolved $\mu_{eff}$ variation model in Step 4 are physics-based operations, proving the high accuracy of the proposed $R_{on,dy}$ model.

## IV. Conclusion

In this letter, physics based SPICE models incorporating $R_{on,dy}$ variations of p-GaN HEMTs are proposed. Experimental and simulative results indicate that the simulations of $R_{on,dy}$ are successfully achieved during switching operations. The model is proposed based on the mechanisms behind $R_{on,dy}$ and reliability models for trapping effect, meanwhile, the model parameters are extracted by characterizing the traps. Moreover, the proposed time-resolved $\mu_{eff}$ variation model proves the $R_{on,dy}$ vary with working time. Then, incorporating with ASM-HEMT and commercial simulation tool proves the convenience of usage. Finally, the accuracy and superiority of proposed models are validated by experiments and simulative prediction.

## References

[1] M. Najjar, A. Kouchaki, J. Nielsen, R. Dan Lazar, and M. Nymand, "Design procedure and efficiency analysis of a 99.3% efficient 10 kW three-phase three-level hybrid GaN/Si active neutral point clamped converter," *IEEE Trans. Power Electron.*, vol. 37, no. 6, pp. 6698–6710, Jun. 2022, doi: 10.1109/TPEL.2021.3131955.

[2] A. M. Naradhipa, S. Kim, D. Yang, S. Choi, I. Yeo, and Y. Lee, "Power density optimization of 700 kHz GaN-based auxiliary power module for electric vehicles," *IEEE Trans. Power Electron.*, vol. 36, no. 5, pp. 5610–5621, May 2021, doi: 10.1109/TPEL.2020.3026328.

[3] S. Mukherjee, J. M. Ruiz, and P. Barbosa, "A high power density wide range DC-DC converter for universal electric vehicle charging," *IEEE Trans. Power Electron.*, vol. 38, no. 2, pp. 1998–2012, Feb. 2022, doi: 10.1109/TPEL.2022.3217092.

[4] F. Yang, S. Dalcanale, M. Gajda, S. Karboyan, M. J. Uren, and M. Kuball, "The impact of hot electrons and self-heating during hard-switching in AlGaN/GaN HEMTs," *IEEE Trans. Electron Devices*, vol. 67, no. 3, pp. 869–874, Mar. 2020, doi: 10.1109/TED.2020.2968212.

[5] E. Fabris et al., "Hot-electron trapping and hole-induced detrapping in GaN-based GITs and HD-GITs," *IEEE Trans. Electron Devices*, vol. 66, no. 1, pp. 337–342, Jan. 2019, doi: 10.1109/TED.2018.2877905.

[6] S. Yang, C. Zhou, S. Han, J. Wei, K. Sheng, and K. J. Chen, "Impact of substrate bias polarity on buffer-related current collapse in AlGaN/GaN-on-Si power devices," *IEEE Trans. Electron Devices*, vol. 64, no. 12, pp. 5048–5056, Dec. 2017, doi: 10.1109/TED.2017.2764527.

[7] G. Zulauf, M. Guacci, J. M. Rivas-Davila, and J. W. Kolar, "The impact of multi-MHz switching frequencies on dynamic on-resistance in GaN-on-Si HEMTs," *IEEE Open J. Power Electron.*, vol. 1, pp. 210–215, Jul. 2020, doi: 10.1109/OJPEL.2020.3005879.

[8] G. Zulauf, M. Guacci, and J. W. Kolar, "Dynamic on-resistance in GaN-on-Si HEMTs: Origins, dependencies, and future characterization frameworks," *IEEE Trans. Power Electron.*, vol. 35, no. 6, pp. 5581–5588, Jun. 2020, doi: 10.1109/TPEL.2019.2955656.

[9] C. Kuring, M. Tannhaeuser, and S. Dieckerhoff, "Improvements on dynamic on-state resistance in normally-off GaN HEMTs," in *Proc. Int. Exhib. Conf. Power Electron., Intell. Motion, Renewable Energy Energy Manage.*, 2019, pp. 1–8.

[10] S. Karboyan, M. J. Uren, J. W. P. Manikant, and M. Kuball, "On the origin of dynamic Ron in commercial GaN-on-Si HEMTs," *Microelectron. Rel.*, vol. 81, pp. 306–311, 2018, doi: 10.1016/j.microrel.2017.10.006.

[11] M. C. J. Weiser, J. Hückelheim, and I. Kallfass, "A novel approach for the modeling of the dynamic ON-state resistance of GaN-HEMTs," *IEEE Trans. Electron Devices*, vol. 68, no. 9, pp. 4302–4309, Sep. 2021, doi: 10.1109/TED.2021.3098498.

[12] O. C. Spro, D. Peftitsis, O.-M. Midtgard, and T. Undeland, "Modelling and quantification of power losses due to dynamic on-state resistance of GaN E-mode HEMT," in *Proc. IEEE 18th Workshop Control Model. Power Electron.*, 2017, pp. 1–6, doi: 10.1109/COMPEL.2017.8013410.

[13] K. Li, P. L. Evans, C. M. Johnson, A. Videt, and N. Idir, "A GaN-HEMT compact model including dynamic RDSon effect for power electronics converters," *Energies*, vol. 14, no. 8, Apr. 2021, Art. no. 2092, doi: 10.3390/en14082092.

[14] K. Li, P. L. Evans, and C. M. Johnson, "Characterisation and modeling of gallium nitride power semiconductor devices dynamic on-state resistance," *IEEE Trans. Power Electron.*, vol. 33, no. 6, pp. 5262–5273, Jun. 2018, doi: 10.1109/TPEL.2017.2730260.

[15] F. Yang, C. Xu, E. Ugur, S. Pu, and B. Akin, "Design of a fast dynamic on-resistance measurement circuit for GaN power HEMTs," in *Proc. IEEE Transp. Electrific. Conf. Expo.*, 2018, pp. 359–365, doi: 10.1109/ITEC.2018.8450093.

[16] P. Cui et al., "Effect of polarization coulomb field scattering on electrical properties of the 70-nm gate-length AlGaN/GaN HEMTs," *Sci. Rep.*, vol. 8, Aug. 2018, Art. no. 12850, doi: 10.1038/s41598-018-31313-9.

[17] A. Zhang et al., "Reliability variability simulation methodology for IC design: An EDA perspective," in *Proc. IEEE Int. Electron Devices Meeting*, 2015, pp. 11.5.1–11.5.4, doi: 10.1109/IEDM.2015.7409677.

[18] S. Khandelwal et al., "ASM GaN: Industry standard model for GaN RF and power devices," *IEEE Trans. Electron. Devices*, vol. 66, no. 1, pp. 80–86, Jan. 2019.

[19] "Datasheet of PowerExpert," Julin Technology, 2022. [Online]. Available: https://julin-tech.com.cn/product/67.html

[20] K. Tanaka, M. Ishida, T. Ueda, and T. Tanaka, "Effects of deep trapping states at high temperatures on transient performance of AlGaN/GaN heterostructure field-effect transistors," *Japanese J. Appl. Phys.*, vol. 52, no. 42, pp. 04CF07.1–04CF07.5, Mar. 2013,.

[21] "Test method guidelines for GaN HEMT based power conversion devices, version 1.0, JEP173," JEDEC PUBLICATION, Dynamic ON-Resistance. Jan. 2019. [Online]. Available: https://www.jedec.org/standards-documents/docs/jep173